Graphite Sublimation Chemistry Nonequilibrium Effects

R. L. Baker*
The Aerospace Corporation, Los Angeles, Calif.

The implications of the assumption of local solid-gas phase equilibrium for subliming carbon species for graphite ablation calculations in an air environment is investigated. The equilibrium assumption is eliminated by considering the Knudsen-Langmuir equation at the interface for each carbon species. Calculated equilibrium and nonequilibrium results are compared for a very wide range of flight and ground-test environments. The nonequilibrium mass addition parameter is always less than the equilibrium value, and the nonequilibrium wall temperature is always larger for a given environment. Calculations made to determine the convective heat flux required to reach an incipient melt temperature of 3800 K indicate that the required flux determined from an equilibrium calculation can be too high by as much as 200-300% for stagnation enthalpies less than 5000 Btu/lb. Calculations for superorbital re-entry conditions show large differences in the mass addition parameter B' when the convective heating rate is low and the external radiation heating level is relatively high. Similar large differences in B' could be simulated in an existing ground-test facility if the reported external radiation heating level could be increased. Such an experiment would provide data to test the validity of present convective-heating-rate blowing correlations in a combined heating environment.

Introduction

IN the formulation of problems involving interphase transfer of mass, it is necessary to relate the concentrations of the principal mass transfer species in one phase to their concentrations in the other phase. For graphite ablation calculations, the carbon species concentrations in the gas phase are proportional to the partial pressures of each species at the solid-gas interface. Practically all graphite ablation calculations are made by assuming that the partial pressure p_i of carbon species i at the wall is equal to the vapor pressure p_i^v of that species at the wall temperature.[1-3] In order for this to be true, the solid and the gas phase must be in equilibrium with one another at the wall temperature. If the solid and the gas phase are in equilibrium at the wall temperature, then the same number of molecules are condensing from the gas phase into the solid as those vaporizing from the solid into the gas. This means that there is no net transfer of mass between phases; therefore, we know the assumption that $p_i = p_i^v$ cannot be exact for finite interphase mass transfer rates.

The purpose of this work is to formulate the graphite ablation problem without making the assumption that $p_i = p_i^v$ and to determine the implications of this simplifying assumption for an air environment by comparison of results calculated using both methods. In the remaining discussion, the problem formulation with p_i assumed equal to p_i^v at the wall temperature simply is termed equilibrium. When this assumption is not made, the term nonequilibrium formulation is used.

Problem Formulation

Knudsen-Langmuir Equation

It can be shown from kinetic theory[4] that the mass of gaseous species i striking a unit area of wall per sec is given by

$$\mu_i = \sqrt{\mathfrak{M}_i/2\pi RT_w}\; p_i \tag{1}$$

where T_w is the wall temperature, $\mathfrak{M}_i$ is the molecular weight of species i, and p_i is the pressure. By referring to Fig. 1, we find that similar expressions can be written for the mass vaporizing from the solid and condensing from the gas phase per unit area per second. Then a simple interphase mass balance gives the following expression for the net transfer of mass per unit area per second between phases:

$$\dot{m}_i = \alpha_i \sqrt{\mathfrak{M}_i/2\pi RT_w}\; (p_i^v - p_i) \tag{2}$$

This equation is the Knudsen-Langmuir equation.[4] The p_i^v and p_i are the vapor pressure of species i at the wall temperature T_w, and the partial pressure of species i, one mean free path from the wall. These pressures cannot be equal to one another if there is to be any net interphase transfer of mass. The coefficient α_i in Eq. (2) is the vaporization coefficient. From kinetic theory, the maximum mass flux vaporizing per unit area of wall per second is $\sqrt{\mathfrak{M}_i/2\pi RT_w}\; p_i^v$. The actual mass flux is $\alpha_i \sqrt{\mathfrak{M}_i/2\pi RT_w}\; p_i^v$. The value of α_i must be determined experimentally. In obtaining Eq. (2), it has been assumed that the vaporization coefficient and the condensation coefficient are equal (see Fig. 1). Equation (2) represents a surface mass balance on a microscopic or molecular level.

Mass Conservation Equation: Binary System

The principal equations used in defining the present problem are the macroscopic mass and energy conservation equations. As shown by Kubota,[5] modeling of the convective and diffusive mass fluxes at the wall (see Fig. 2) gives the

$$\dot{m} = \dot{m}_{vap} - \dot{m}_{cond}$$

$$\dot{m} = \sqrt{\frac{\mathfrak{M}_i}{2\pi RT_w}}\left[\alpha_{vap} p_i^v - \alpha_{cond} p_i\right]$$

$$\dot{m} = \alpha_i \sqrt{\frac{\mathfrak{M}_i}{2\pi RT_w}}\left[p_i^v - p_i\right] \quad \text{FOR } \alpha_i = \alpha_{vap} = \alpha_{cond}$$

$$\dot{m}_{cond} = \alpha_{cond} \sqrt{\frac{\mathfrak{M}_i}{2\pi RT_w}}\, p_i \qquad \dot{m}_{vap} = \alpha_{vap} \sqrt{\frac{\mathfrak{M}_i}{2\pi RT_w}}\, p_i^v$$

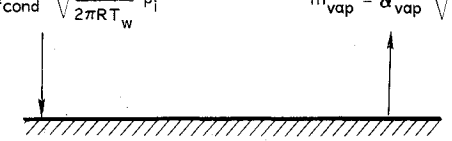

Fig. 1 Microscopic surface mass balance.

Presented as Paper 75-735 at the AIAA 10th Thermophysics Conference, Denver, Colo., May 27-29, 1975; submitted May 23, 1977.

Index categories: Ablation, Thermochemistry and Chemical Kinetics.

*Member of Technical Staff, Fluid Mechanics Department. Member AIAA.

$$\dot{m} = \dot{m}_{conv} + \dot{m}_{diff}$$

$$\dot{m} = (\rho v)_w K_{i_w} + \rho_e u_e C_H K_{i_w}$$

$$\dot{m} = \dot{m} K_{i_w} + \rho_e u_e C_H K_{i_w}$$

$$B' = \frac{\dot{m}}{\rho_e u_e C_H} = \frac{K_{i_w}}{1 - K_{i_w}}$$

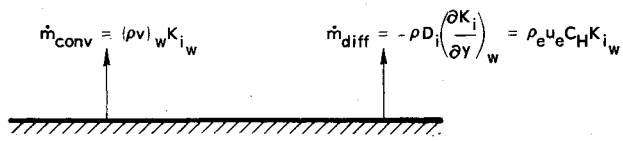

Fig. 2 Macroscopic surface mass balance.

following relationship between the mass addition parameter B' and the mass fraction of vaporizing species at the wall, K_{l_w}, for unity value of Lewis and Prandtl numbers:

$$B' = K_{l_w} / (1 - K_{l_w}) \tag{3}$$

K_{l_w} is related to the partial pressure at the wall p_l and the molecular weight $\mathfrak{M}_l$ of the vaporizing species by the relationship $K_l = p_l \mathfrak{M}_l / p_e \overline{\mathfrak{M}}$, where p_e is the pressure at the edge of the boundary layer and $\overline{\mathfrak{M}}$ is the average molecular weight of the gas at the wall. Making this substitution into Eq. (3) and simplifying for a binary system of components 1 and 2 results in the following equation for the mass addition parameter B':

$$B' = \{ (\mathfrak{M}_2 / \mathfrak{M}_l) [(p_e / p_l) - 1] \}^{-1} \tag{4}$$

In the equilibrium formulation, it is assumed that $p_l = p_l^v$, leading to the well-known relationship

$$B'_{eq} = \frac{(\mathfrak{M}_l / \mathfrak{M}_2)(p_l^v / p_e)}{[1 - (p_l^v / p_e)]} \tag{5}$$

For the nonequilibrium formulation, the p_l is obtained from the Knudsen-Langmuir relationship, Eq. (2). Thus, if Eqs. (2) and (3) are combined, p_l and p_l^v are related by

$$p_l = \frac{p_l^v}{\left[1 + \dfrac{\sqrt{2\pi R T_w \mathfrak{M}_l}\, \rho_e u_e C_H (B' + 1)}{\alpha_l \overline{\mathfrak{M}} p_e}\right]} \tag{6}$$

where $\rho_e u_e C_H$ is the heat-transfer coefficient.

For $\dot{m} / \alpha_l \mu_l \ll 1$, Eqs. (1, 2, and 4) may be combined to give the following approximate expression for the reduction in B'_{eq} due to nonequilibrium effects:

$$B' = B'_{eq} [1 - (\dot{m} / \alpha_l \mu_l)] \tag{7a}$$

For the binary system presently being considered, the $\overline{\mathfrak{M}}$ in Eq. (6) can be written in terms of $\mathfrak{M}_l$, $\mathfrak{M}_2$, p_l, and p_e. This expression then can be combined with Eq. (4) to give the following approximate relationship between B' and B'_{eq} for $\sqrt{2\pi R T_w \mathfrak{M}_l}\, \rho_e u_e C_H / \alpha_l \mathfrak{M}_2 p_e \ll 1$:

$$B' = B'_{eq} \left\{ \frac{1 - [\sqrt{2\pi R T_w \mathfrak{M}_l}\, \rho_e u_e C_H] / \alpha_l \mathfrak{M}_2 p_e}{1 + B'_{eq} [\sqrt{2\pi R T_w \mathfrak{M}_l}\, \rho_e u_e C_H] / \alpha_l \mathfrak{M}_2 p_e} \right\} \tag{7b}$$

Equations (7a) and (7b) both are obtained by expanding in a binomial series and retaining the first two terms. From Eqs. (7a) and (7b), we see that the nonequilibrium value of the mass addition parameter B' is always less than the equilibrium value B'_{eq}. The degree of departure from equilibrium is proportional to $\dot{m}/\mu_l$, or $\rho_e u_e C_H / p_e$, and inversely proportional to α_l. As the net transfer rate of mass between phases $\dot{m}$ increases relative to the rate of mass striking the wall μ_l, nonequilibrium effects increase. The ratio $\dot{m}/\mu_l$ is proportional to $\rho_e u_e C_H / p_e$, so that maximum nonequilibrium effects will be seen when large heat-transfer coefficients occur at low pressures.

Mass Conservation Equation: Multiple Species

The aforementioned equations were restricted to a binary system with no surface chemistry other than the vaporization or sublimation process. For graphite ablation, it is necessary to consider multiple carbon species at the wall as well as chemical reaction of the carbon with the freestream gas. Equation (3) for graphite ablation becomes[6]

$$B' = (\Sigma K_{i_w} + F_O + F_N) / (1 - \Sigma K_{i_w} - F_N) \tag{8a}$$

where F_O and F_N result from the carbon-oxygen and carbon-nitrogen chemical reactions, respectively. The mass fractions K_{i_w} now enter as a summation over all carbon species i.

The functions F_O and F_N are given by

$$F_O = (\mathfrak{M}_C / \mathfrak{M}_O) \tilde{K}_{O_e}$$

$$F_N = \left[\frac{\mathfrak{M}_C}{\mathfrak{M}_{CN}} K_{CN} + \frac{\mathfrak{M}_{C_2}}{\mathfrak{M}_{C_2N_2}} K_{C_2N_2} + \frac{\mathfrak{M}_{C_4}}{\mathfrak{M}_{C_4N_2}} K_{C_4N_2} \right]_w$$

where $\tilde{K}_{O_e}$ for air is 0.232. The carbon-nitrogen compound mass fractions at the wall were calculated assuming gas phase chemical equilibrium. This simplifying assumption is justified by the very small (<5% of total) surface mass loss associated with nitrogen chemistry. The equilibrium constants were obtained from Dow Chemical.[7] The mass fractions K_{i_w} again may be related to the partial pressures p_i and the molecular weights $\mathfrak{M}_i$. Therefore, B' may be written

$$B' = [\Sigma p_i \mathfrak{M}_i + p_e \overline{\mathfrak{M}} (F_O + F_N)] / [p_e \overline{\mathfrak{M}} (1 - F_N) - \Sigma p_i \mathfrak{M}_i] \tag{8b}$$

Equation (8b) is applicable in general. For the equilibrium case, the p_i's are given by the individual p_i^v at the wall temperature. For the nonequilibrium case, a carbon species mass balance at the wall gives

$$\dot{m}_i = [\dot{m} + \rho_e u_e C_H] K_i \tag{9}$$

Combination of Eqs. (2) and (9) then gives the following expression for p_i:

$$p_i = \frac{p_i^v}{\left[1 + \dfrac{\sqrt{2\pi R T_w \mathfrak{M}_i}\, \rho_e u_e C_H (B' + 1)}{\alpha_i \overline{\mathfrak{M}} p_e}\right]} \tag{10}$$

$$\dot{q}_c = \dot{q}_{diff} - \dot{q}_{conv} - \dot{q}_r + \dot{q}_{ext}$$

$$\dot{q}_c = \rho_e u_e C_H \left[H^o - H_w\right] - \dot{m}\left[H_w - H_s\right] - \epsilon\sigma T_w^4 + \dot{q}_{ext}$$

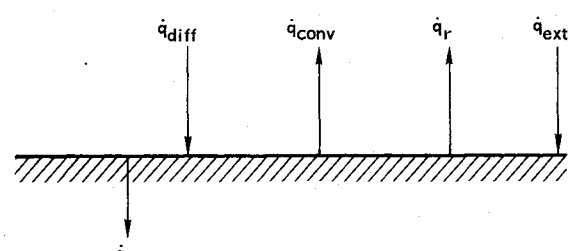

Fig. 3 Macroscopic surface energy balance.

Equation (10) is the same as Eq. (6) with the subscript *1* replaced by the subscript *i*. The only assumption made in obtaining Eq. (10) is that the $\dot{m}_i$ in Eq. (9) is the same as the $\dot{m}_i$ in Eq. (2); i.e., the carbon species at the wall are frozen. The sensitivity of results to this assumption is examined in the discussion of results. Since the $\overline{\mathfrak{M}}$ in Eq. (10) depends on $\Sigma p_i m_i$, an iterative calculation procedure is required.

The values of α_i used in Eq. (10) were, except in the sensitivity study, the "nominal values" given by Dolton, et al.[1], i.e., $\alpha_1 = 0.24$, $\alpha_2 = 0.5$, $\alpha_3 = 0.023$, $\alpha_4 = 0.25$, $\alpha_5 = 0.0019$. All of the calculations presented here were obtained using the carbon species thermochemical data of Palmer and Shelef[4] to calculate p_i^v for species C_1 through C_5 (see appendix).

Energy Conservation Equation

As shown in Fig. 3, the energy conservation equation at the interface can be written

$$\dot{q}_c = \rho_e u_e C_H (H^o - H_w) - \dot{m}(H_w - H_s) - \epsilon\sigma T_w^4 + \dot{q}_{ext} \quad (11)$$

where $\dot{q}_c$ and $\dot{q}_{ext}$ are the net conduction heat flux into the body and the external radiation heat flux; H^o, H_w, and H_s are the stagnation enthalpy, the enthalpy of the gas at the wall, and the enthalpy of the solid at the wall; $\dot{m}$ is the total mass flux of ablating species; and $\epsilon\sigma T_w^4$ is the radiation heat flux away from the wall.

Nonequilibrium effects are contained implicitly in the energy equation through effects on the ratio, $\dot{m}/\rho_e u_e C_H$ (i.e., B') and on H_w, which is evaluated based upon p_i instead of on p_i^v.

Primary Dependent and Independent Variables

Equations (8) and (11) provide two equations in the primary dependent variables B' and H_w. Solving these equations together satisfies the surface mass and energy conservation equations simultaneously and provides a unique value of B' and H_w. For the equilibrium case, both B' and H_w are functions of the edge pressure p_e and the wall temperature T_w. If the steady-state ablation assumption is made, i.e., $\dot{q}_c = \dot{m}(H_s - H_b)$, Eq. (11) may be written

$$\frac{B'(H_w - H_b) + H_w}{H^o} + \frac{\epsilon\sigma T_w^4 (C_{H_0}/C_H)}{\dot{q}_{cw}} = 1 \quad (12a)$$

where the substitution $\rho_e u_e C_H H^o = \dot{q}_{cw}(C_H/C_{H_0})$ has been made. The term H_b is the bulk enthalpy of the solid and $\dot{q}_{cw}$ is the cold-wall convective heat flux.

Usually the blowing correction C_H/C_{H_0} is written as a function of B'. [All calculations reported in this work were based upon laminar correction to the Stanton number to account for surface blowing effects. The relationship used is $C_H/C_{H_0} = \ell n(1.28B' + 1)/1.28B'$ (Ref. 14).] Thus, functionally, Eq. (12a) may be written

$$[F_1(p_e, T_w)/H^o] + [F_2(p_e, T_w)/\dot{q}_{cw}] = 1 \quad (12b)$$

Writing the energy balance equation in this way was suggested first by Kendall.[8] Equation (12b) provides valuable insight into the determination of the independent variables. The edge pressure p_e is a primary independent variable. The wall temperature T_w, although an independent variable, is implicit; the other variables $\dot{q}_{cw}$ and H^o are not independent, but rather related to one another by Eq. (12b). If the value of B' (and therefore of T_w) is fixed at a given pressure p_e, Eq. (12b) may be written

$$(A/H^o) + (B/\dot{q}_{cw}) = 1 \quad (12c)$$

where A and B are constants. Thus, the selected value of B' will be obtained (at the pressure p_e) for all combinations of H^o and $\dot{q}_{cw}$, satisfying Eq. (12c). A graphical solution procedure based upon this, which allows the determination of B' for given p_e, H^o, and $\dot{q}_{cw}$ using a single graph, was given by Rindal et al.[8] In summation, for the equilibrium case, B' may be regarded as a function of p_e, H^o, and $\dot{q}_{cw}$. For fixed p_e, a given value of B' is obtained for all H^o, and $\dot{q}_{cw}$, satisfying Eq. (12c). This is illustrated in Table 1. For a pressure of 0.1 atm, $B' = 0.420$ for all of the H^o, $\dot{q}_{cw}$ combinations given, since all of them satisfy Eq. (12c). Note that the wall temperature is the same for all cases, also as required. The independent variables for the nonequilibrium case are discussed in the next section.

Discussion of Results

Nature of Nonequilibrium Effects

Initially to illustrate differences in results calculated using the equilibrium and the nonequilibrium formulation, it is informative to make such a comparison for a series of environmental parameters for which the equilibrium mass addition parameter is a constant. If the previous discussion of dependent and independent variables is recalled, the $\dot{q}_{cw}$, H^o conditions in Table 1 all give a value of B' (equilibrium assumption) of 0.420. Therefore, let us compare nonequilibrium calculated results with the equilibrium results in Table 1. These comparisons are shown in Fig. 4. All of the calculated equilibrium results are given by the single point indicated by an X on the equilibrium B' curve. Calculated nonequilibrium results have a B' less than the equilibrium value and a wall temperature greater than when solid-gas equilibrium is assumed. The reduction in B', caused by p_i being less than p_i^v [see Eq. (10)], reaches a reasonably constant value. However, the surface temperature continues to increase over its equilibrium value as H^o is decreased, and $\dot{q}_{cw}$ increases, i.e., as $\rho_e u_e C_H$ increases. For the equilibrium case, the independent variables were shown to be p_e with all combinations of $\dot{q}_{cw}$ and H^o satisfying Eq. (12c). From Fig. 4 we see that for the nonequilibrium case, p_e, H^o, and $\dot{q}_{cw}$ are all independent variables by themselves.

The sensitivity of nonequilibrium calculated results to the numerical values of the vaporization coefficients is shown in Table 2. The six cases considered are the same as those discussed in Table 1 and Fig. 4. Results for the nominal values of α_i are given in the third column. Increasing all the values of α_i to unity gives results very close to the equilibrium values in Table 1. Increasing only α_3 to unity is about the same as increasing all the values of α_i. Decreasing all values of α_i to 0.01 decreases B' below that for the nominal values of α_i for $H^o \geq 10{,}000$ and increases the wall temperature for all H^o. The importance of nonequilibrium effects thus depends upon the validity of the relatively low value of α_3, i.e., $\alpha_3 = 0.023$. If $\alpha_3 = 1.0$, nonequilibrium effects on B' are minimal, and the maximum increase in wall temperature over the equilibrium calculated temperatures is about 200 K.

The sensitivity of nonequilibrium calculated results to the frozen assumption made in the derivation of Eq. (10) was examined briefly by substituting the gas phase equilibrium equation

$$p_i/p_i^v = (p_j/p_j^v)^{i/j}$$

Table 1 Equilibrium B' values

p_e, atm	$\dot{q}_{cw}$, Btu/ft^2-sec	H^o Btu/lb	T_w, K	B'
0.1	605	100,000	3281	0.420
0.1	647	40,000	3281	0.420
0.1	734	20,000	3281	0.420
0.1	1000	10,000	3281	0.420
0.1	3646	5000	3281	0.420
0.1	13,112	4400	3281	0.420

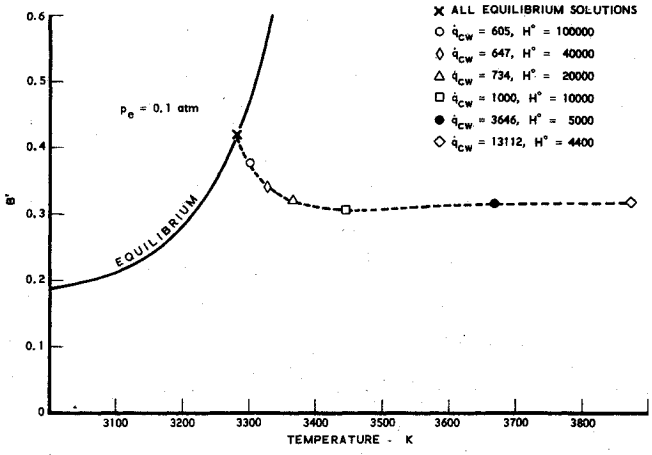

Fig. 4 Differences between equilibrium and nonequilibrium solutions.

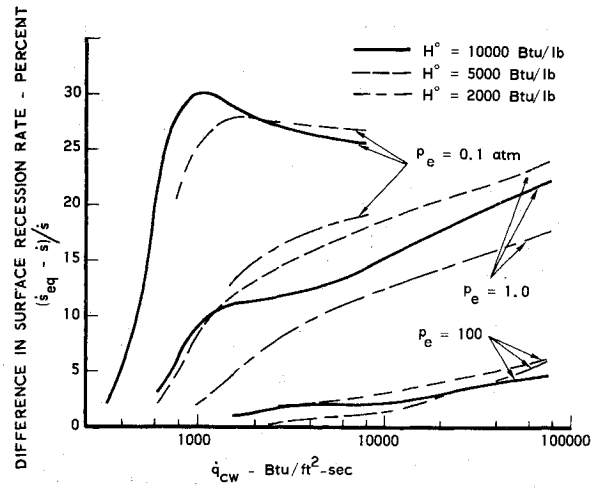

Fig. 6 Nonequilibrium effect on surface recession rate.

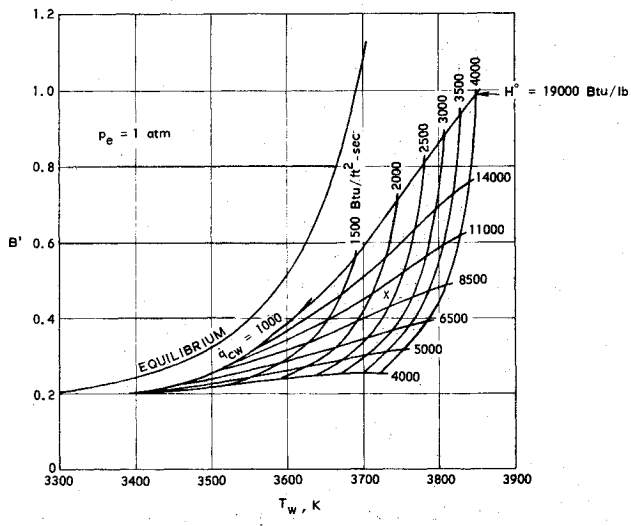

Fig. 5 Nonequilibrium effects on B' and T_w.

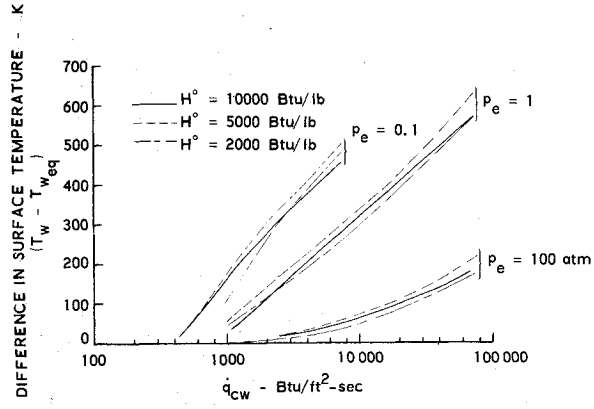

Fig. 7 Nonequilibrium effect on surface temperature.

in place of Eq. (10). Limited calculations indicated results very similar to those obtained using Eq. (10).

Graphical Solution Procedure

All solutions for the equilibrium case can be represented on a single graph using the method of Rindal et al.[8] However, since there are three independent variables in the nonequilibrium case, there is no convenient way of representing all solutions on a single graph. For a given pressure p_e there is a unique value of B' and T_w for specified H^o and $\dot{q}_{cw}$ as shown in Fig. 4. This suggests that for given p_e, a convenient way of graphically presenting results would be to plot lines of constant H^o and constant $\dot{q}_{cw}$ in the same B', T_w plane as in Fig. 4. Such a plot for an edge pressure p_e of 1 atm is shown in Fig. 5. For this pressure, Fig. 5 gives B' values and surface temperatures for $\dot{q}_{cw}$ ranging from 1000 to 4000 Btu/ft^2-sec and for H^o values of 4000 to 19,000 Btu/lb. To use Fig. 5, one interpolates in the "spider web" region for the $\dot{q}_{cw}$ and H^o of interest. For instance, for $\dot{q}_{cw}$ equal to 2300 Btu/ft^2-sec and H^o equal to 10,000 Btu/lb, the B' and T_w of approximately 0.462 and 3730 K, respectively, are indicated by the small x. A plot such as Fig. 5 would be useful, for instance, for graphite arc jet ablation results at constant pressure where the stagnation enthalpy H^o and the cold wall heat flux $\dot{q}_{cw}$ are varied by changing the arc current and the body geometry.

Mass Loss and Surface Temperature Differences for Typical Re-entry Vehicle Environments

Nonequilibrium calculations have been shown to result in lower values of B' and higher wall temperatures. The surface

Table 2 Effect of α_i values on nonequilibrium results

$\dot{q}_{cw}$,	H^o	Nominal α_i i=1-5		$\alpha_i = 1.0$ i=1-5		$\alpha_i = 0.01$ i=1-5		$\alpha_3 = 1.0$ Other α_i nom.		$\alpha_3 = 0.01$ Other α_i nom.	
Btu/ft-sec	Btu/lb	B'	T_w	B'	T_w	B'	T_w	B'	T_w	B'	T_w
605	100,000	0.376	3302	0.419	3281	0.342	3319	0.415	3284	0.343	3317
647	40,000	0.348	3327	0.418	3282	0.298	3358	0.412	3285	0.304	3351
734	20,000	0.320	3367	0.416	3285	0.277	3416	0.411	3289	0.284	3398
1000	10,000	0.307	3443	0.411	3294	0.276	3532	0.408	3299	0.282	3478
3646	5000	0.315	3670	0.404	3365	0.323	3854	0.405	3377	0.302	3708
13,112	4400	0.317	3873	0.396	3484	0.342	4088	0.400	3503	0.306	3914

recession rate $\dot{s}$ is obtained from B' through the relationship

$$\rho_b \dot{s} = (B' \dot{q}_{cw}/H^o)(C_H/C_{H_0})$$

where ρ_b is the bulk density of the ablating material. Quantitative results showing the differences in the calculated surface recession rate $\dot{s}$ and the surface temperature T_w for a wide range of re-entry environments are shown in Figs. 6 and 7. For stagnation enthalpies of 2000, 5000, and 10,000 Btu/lb, pressures from 0.1 to 100 atm, and cold-wall heating values from 300 to 75,000 Btu/ft^2-sec, Fig. 6 shows that the difference in the calculated recession rate due to the equilibrium assumption is never greater than 30%. The corresponding differences in the surface temperature, shown in Fig. 7, range up to a maximum of about 600 K, obtained when the equilibrium surface temperature is predicted to be about 3400 K; whereas the calculated nonequilibrium temperature is about 4000 K. In both Figs. 6 and 7 we see that the largest differences occur at lower pressures (with larger $\rho_e u_e C_H$), where the ratio of the interphase mass-transfer rate to the collision frequency at the wall is largest. These differences are of the same order as those due to the assumption of alternate carbon-species thermochemistry models.[9] Since over 90% of the total recession occurs at pressures greater than 10 atm for typical re-entry trajectories, it can be seen from Fig. 6 that the difference in the total integrated recession will be on the order of 5 to 10% maximum. Thus, the added complexity of the nonequilibrium formulation is not justified for re-entry vehicle nosetip-surface-recession predictions. However, a 600 K difference in the surface temperature may not be tolerable for thermostructural design purposes.

Graphite Melt Considerations

The question of whether graphite will melt under re-entry vehicle convective heating environments has been considered by Rindal and Powars[16] and by Kratsch.[10] These authors conclude that for high-beta re-entry vehicle trajectories it is possible, for small nose radii (¼ to ½ in.), to reach an assumed melt temperature in the range of 4000 to 4200 K.

The equations described in this work are applicable up until the time that the wall temperature reaches the melt temperature. When the melt temperature is reached, additional modeling of the melt layer on the surface is required.

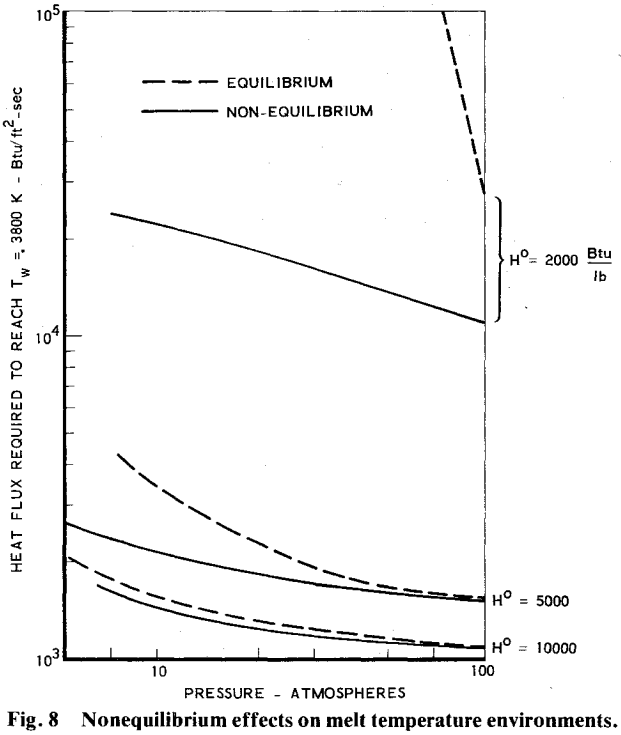

Fig. 8 Nonequilibrium effects on melt temperature environments.

Equilibrium and nonequilibrium calculations were performed to determine differences in the heat flux required to reach an incipient melt temperature of 4200 K at a pressure of 100 atm for stagnation enthalpies of 2000, 5000, and 10,000 Btu/lb. For $H^o = 10{,}000$ Btu/lb, the required heat flux values from the equilibrium and nonequilibrium formulations were 3000 and 2750 Btu/ft^2-sec, respectively. For $H^o = 5000$ Btu/lb, the corresponding required heat flux values were 21,700 and 6700 Btu/ft^2-sec. Thus, melting could occur at this stagnation enthalpy, based upon the nonequilibrium calculation. However, the required equilibrium calculation value of $\dot{q}_{cw}$ is over 300% larger and could not be obtained at this enthalpy.

A melt temperature for graphite in the range 4000-4200 K is not accepted universally. There is some old[11] as well as some very recent[12] evidence that the melt temperature is about 3800 K, and that the triple-point pressure is closer to 1 atm than to 100 atm. Therefore, calculations like those just mentioned were made for an incipient melt temperature of 3800 K for pressures ranging from 10 to 100 atm. The results are shown in Fig. 8. The difference in the calculated heat flux required to attain incipient surface melting is quite small over the whole range of pressure for $H^o = 10{,}000$ Btu/lb. For $H^o = 5000$ Btu/lb, the equilibrium prediction for heat flux is 50% too high at lower pressures. For ground-test environments with stagnation enthalpies in the range 2000-5000 Btu/lb, differences of over 200% can occur, even at a pressure of 100 atm.

These results indicate that very large differences in the predicted heating environment required to reach incipient melt conditions can occur when the solid-gas equilibrium assumption is made. Once the melt temperature is reached, the liquid graphite has a vaporization rate (B') much greater than the solid graphite.[10,11] Because of this, essentially 100% of the liquid melt layer is vaporized and very little is stripped off as liquid. Thus, nearly full advantage still may be taken of the very large amount of heat required to change solid graphite to gaseous species in the boundary layer. However, when the surface temperature has reached the melt temperature, the modeling must be changed to account for the presence of liquid graphite as done by Kratsch.[10] No attempt was made to carry out this type of modeling in the present work.

Radiation Heating Effects

Results presented thus far have been restricted to a convective heating environment for ground-test or flight applications. If the freestream velocity is increased from reentry vehicle values like 25,000 fps to superorbital velocities like 50,000 fps, gas cap radiation heating to the solid surface becomes important, in addition to the convective heating. Graphite ablation predictions for an Apollo-type vehicle reentering the Earth's atmosphere at superorbital velocities have been made by Bartlett et al.[13]

Equilibrium and nonequilibrium calculations were made for the range of convective and radiation heating levels given.[13] The particular conditions chosen were an altitude of 220,000 ft and a velocity of 45,000 fps, which result in a stagnation pressure of 0.23 atm and a stagnation enthalpy of 40,318 Btu/lb. The calculated results are summarized in Table 3. The surface temperature difference is quite small over the whole range of conditions. The surface recession rate difference is small until the condition of low convective-heating rate and higher radiation-heating rate associated with larger nose radii is approached. For these heating conditions, the calculated B'_{eq} may be nearly twice the nonequilibrium value, with both B' and B'_{eq} becoming significantly greater than one, i.e., massive blowing. Despite the large difference in B', the difference in the predicted recession rate $\dot{s}$ is only about 25%, because of a compensating effect associated with the blowing correction to the convective heating rate. [When the equilibrium B' is much larger than the nonequilibrium B', C_H/C_{H_0} is much less for the equilibrium case. Since $\rho_b \dot{s} = B'$

Table 3 Superorbital re-entry calculations

p_e, atm	H^o, Btu/lb	$\dot{q}_{cw}$, Btu/ft^2-sec	$\dot{q}_{ext}$, Btu/ft^2-sec	$T_w - T_{w_{eq}}$, K	B'	$\frac{B'_{eq} - B'}{B'}$	$\frac{\dot{s}_{eq} - \dot{s}}{\dot{s}}$
0.23	40,318	2503	106	157	1.98	0.232	0.122
0.23	40,318	1823	166	125	1.70	0.225	0.124
0.23	40,318	1191	290	88	1.44	0.220	0.128
0.23	40,318	851	426	67	1.41	0.222	0.130
0.23	40,318	596	585	51	1.64	0.236	0.131
0.23	40,318	356	825	41	3.32	0.338	0.146
0.23	40,318	237	975	42	9.88	0.746	0.201

Table 4 Large B' in a ground test environment

p_e, atm	H^o, Btu/lb	$\dot{q}_{cw}$, Btu/ft^2-sec	$\dot{q}_{ext}$, Btu/ft^2-sec	$T_w - T_{w_{eq}}$, K	B'	$\frac{B'_{eq} - B'}{B'}$	$\frac{\dot{s}_{eq} - \dot{s}}{\dot{s}}$
0.32[a]	4698	705	1735	181	0.86	0.320	0.209
0.32[a]	4698	705	2193	194	1.18	0.341	0.203
0.32[b]	4698	705	3000	213	1.94	0.389	0.196
0.32[b]	4698	705	5000	256	5.64	0.578	0.195
0.32[b]	4698	705	6000	276	16.0	0.808	0.221

[a] Conditions in experiments of Wakefield.[14] [b] Increased $\dot{q}_{ext}$ above Ref. 14 values.

$(\dot{q}_{cw}/H^o)C_H/C_{H_0}$, the two effects compensate.] Thus, there appear to be no substantial differences in either the wall temperature or the surface recession rate for superorbital re-entry conditions.

The aforementioned statement regarding differences depends intimately upon the validity of the blowing correction to the convective heat-transfer rate in a radiation-augmented heating environment, where B' is being driven to very large values by the external radiation heating. This type of coupling was not present in the data upon which present blowing corrections are based. Thus, it would be desirable to obtain new data in which B' is very large due to external radiation heating. In Table 4, calculated B' and B'_{eq} values for several radiation heating levels at and above those in the ground test experiments of Wakefield[14] are tabulated. From this we see that questions regarding the validity of present blowing corrections to the convective heating rate in highly coupled radiation-convective heating environments could be explored by conducting new ground tests with radiation levels 2 to 3 times higher than those in Wakefield's experiments.

Summary and Conclusions

Comparison of equilibrium and nonequilibrium calculated results for the same environmental conditions indicates that the mass addition parameter, B', is always less and the wall temperature is always greater for the nonequilibrium case. For a given pressure, the difference in B' levels off, and the difference in wall temperature continues to increase as $\dot{q}_{cw}$ increases and H^o decreases, i.e., as the heat-transfer coefficient increases.

For the nonequilbirum case, p_e, H^o, and $\dot{q}_{cw}$ are all independent variables. A convenient graphical solution procedure for a given pressure is to plot lines of constant stagnation enthalpy H^o and lines of constant cold-wall heat flux $\dot{q}_{cw}$ in the B', T_w plane.

Comparison of calculated equilibrium and nonequilibrium results for a wide range of re-entry vehicle environmental conditions indicates a maximum difference in the calculated recession rate of 30% and a maximum difference in the surface temperature of 600 K. The largest differences occur at low pressures for large heat-transfer coefficients. If the graphite melt temperature is 3800 K, then nonequilibrium calculations should be used to determine the heat flux required for incipient melting for stagnation enthalpies less than 5000 Btu/lb, since differences as large as 200 to 300% can occur.

Table 5 Constants from Palmer and Shelef[15]

i	A	B
1	− 85715	18.69
2	− 98363	22.20
3	− 93227	23.93
4	−150307	31.30
5	−133087	32.71

Radiation augmenting of the convective heating environment can cause a dramatic increase in B'. When this happens, differences in B' of over 100% can occur. However, the corresponding difference in the surface recession rate is only about 25%. This effect occurs for superorbital re-entry velocity conditions when the convective heating rate is low and the radiation heating rate is high, i.e., for large nose radii. Ground-test simulation of this effect is possible by increasing the external radiation level of the experiments of Wakefield 2 to 3 times. In this way, experimental determination of the validity of the blowing correction, C_H/C_{H_0}, could be made for a coupled convective-radiation heating environment at the very high B' values of interest.

Appendix: Thermochemistry Data

All of the calculations presented here were obtained using the carbon species C_1 through C_5 thermochemical data of Palmer and Shelef.[4] The values used were termed in that very extensive survey paper the "approximate best." Putting the carbon species vapor pressure equations in the form

$$\ln p_i^v(\text{atm}) = [A/T(^\circ\text{K})] + B \qquad \text{(A1)}$$

the Palmer and Shelef values of A and B[15] are tabulated in Table 5.

Acknowledgment

This study was supported by the Air Force Space and Missile Systems Organization under Contract F04701-74-C-0075. The author is indebted to A.G. Whittaker for bringing to his attention the early data on graphite melt temperature (Ref. 11).

References

[1] Dolton, J.A., Mauer, R.E., and Goldstein, H.E., "Thermodynamic Performance of Carbon in Hyperthermal En-

vironments," AIAA *Progress in Astronautics and Aeronautics, Thermal Design Principles of Spacecraft and Entry Bodies,* Vol. 21, edited by J.T. Bevans, Academic Press, New York, 1969, pp. 169-201.

[2] Kratsch, K.M., Martinez, M.R., Clayton, F.I., Greene, R.B., and Wuerer, J.E., "Graphite Ablation in High Pressure Environments," AIAA Paper 68-1153, Dec. 1968, Williamsburg, Va.

[3] Lundell, J.H. and Dickey, R.R., "Graphite Ablation at High Temperatures," *AIAA Journal,* Vol. 11, Feb. 1973, pp. 216-222.

[4] Palmer, H.B. and Shelef, M., "Vaporization of Carbon," *Chemistry and Physics of Carbon,* Vol. 4, edited by P.L. Walker, Jr., Marcel Dekker, Inc., New York, 1968.

[5] Kubota, T., "Ablation with Ice Model at $M=5.8$," *American Rocket Society Journal,* Vol. 30, Dec. 1960, pp. 1164-1169.

[6] Lees, L., "Convective Heat Transfer with Mass Addition and Chemical Reactions," *Combustion and Propulsion, Third AGARD Colloquium,* 1959, Pergamon Press, New York, pp. 451-498.

[7] *JANAF Thermochemical Tables,* 1969, The Dow Chemical Co., Midland, Mich.

[8] Rindal, R.A., Dahm, T.J., and McVey, D.F., "Graphite Temperature and Ablation Characteristics in Various Environments," AIAA Paper 69-148, New York, Jan. 1969.

[9] Rindal, R.A. and Powars, C.A., "Effects of Carbon Vapor Thermochemistry Uncertainties on R/V Ablation Predictions," AIAA Paper 71-414, Tullahoma, Tenn., April 1971.

[10] Kratsch, K.M., "Graphite Fusion and Vaporization," *ASME/AIAA Tenth Structures, Structural Dynamics and Materials Conference,* Douglas Paper 5338, New Orleans, La., April 1969.

[11] Konig, H., "The Melting of Carbon," *Naturwissenschaften,* Vol. 34, Feb. 1947, pp. 108-111.

[12] Whittaker, A.G. and Kintner, P.L., "Laser-Heating Studies of Carbon Melting and Vaporization," *American Ceramic Society 27th Pacific Coast Regional Meeting,* North Hollywood, Calif., Oct. 23-26, 1974.

[13] Bartlett, E.P., Nicolet, W.E., and Howe, J.T., "Heat-Shield Ablation at Superorbital Re-entry Velocities," *Journal of Spacecraft and Rockets,* Vol. 8, May 1971, pp. 456-463.

[14] Wakefield, R.M. and Peterson, D.L., "Graphite Ablation in Combined Convective and Radiative Heating," *Journal of Spacecraft and Rockets,* Vol. 10, Feb. 1972, pp. 149-154.

[15] Palmer, H.B., Pennsylvania State University, University Park, Penn., personal communication.

[16] Rindal, R.A., "Thermochemical and Thermomechanical Ablation," Air Force Materials Laboratory, Dayton, Ohio, AFML TR 69-73, Vol. IV, Jan. 1970, Appendix D.